

Slip distribution of the 1997 Umbria-Marche earthquake sequence: Joint inversion of GPS and SAR interferometry data

Paul Lundgren

Jet Propulsion Laboratory, California Institute of Technology, Pasadena

Salvatore Stramondo

Istituto Nazionale di Geofisica, Roma, Italy

Abstract: In September-October 1997 a seismic sequence struck the southern part of the Umbria-Marche region in central Italy. The three largest earthquakes took place on September 26 (at 00:33 GMT, M_w 5.7; at 09:40 GMT, M_w 6.0) near the town of Colfiorito, and on October 14 (M_w 5.6) near Sellano. In this paper we present a slip model for the main sequence of events over two separate fault planes. We use previously published Global Positioning System (GPS) and differential interferometric synthetic aperture radar (DInSAR) data as well as new DInSAR data covering the Sellano event as input to a simulated annealing solution for the distribution of fault slip. The combination of both types of geodetic data as well as the combination of SAR interferograms from both ascending and descending satellite tracks allows us to make a more complete geodetically based assessment of the fault slip for these earthquakes. For the solutions presented here we required the slip distribution to match the observed surface displacements while maintaining a total scalar seismic moment approximately equal to the seismologically inferred moments for this sequence. We find the slip was concentrated in a zone at 4-5.5 km depth with a shallower tail extending to near the surface at the northern end of the Colfiorito sequence. For both the second Colfiorito event and the Sellano event individual patches were calculated with maximum slip of 2 meters implying stress drops as high as 20 MPa. Coulomb stress

calculations show that the coseismic slip distribution for the Colfiorito events facilitated slip of the adjacent Sellano earthquake.

1. Introduction

The Umbria-Marche seismic sequence started on September 3, 1997, with an M_w 4.5 earthquake. On September 26 two moderate sized earthquakes of M_w 5.7 (00:33 GMT) and M_w 6.0 (09:40 GMT) [Amato *et al.*, 1998] caused damage to a wide area of central Italy (central Apennines belt). More than two weeks later, on October 14, another earthquake of M_w 5.6 struck the area of Sellano, about 15 km SE of the September 26 events (Plate 1). The seismic sequence had three other events with $M_w > 5.0$ and a great number of smaller aftershocks. The hypocentral depths of the three main events ranged between 4.5-7.0 km, with similar shallow depths found for the aftershock sequence. Surface breaks were present in the epicentral areas as reported by different teams, ranging from a few meters to nearly 1 km in length [Basili *et al.*, 1998; Cello *et al.*, 1998; Cinti *et al.*, 1999]. All three main shocks had purely normal focal mechanisms [Ekström *et al.*, 1998]; the faults are SW dipping with their geometry well constrained by seismological and geological data [Amato *et al.*, 1998; Ekström *et al.*, 1998; Cinti *et al.*, 1999; Basili *et al.*, 1998]. The complexity of this earthquake sequence and its large societal impact for the modest size of the events makes it important to understand the coseismic distribution of slip and their interrelationship.

This earthquake sequence was partially located within an existing Global Positioning System (GPS) network. Only two sites (CROC and PENN) show significant horizontal displacements and only one (CROC) shows significant vertical displacements (Figure 1). When combined with differential interferometric synthetic aperture radar (DInSAR) data,

simple models of the source were computed that give a first order fit to the data [*Stramondo et al.*, 1999; *Salvi et al.*, 2000]. Given the high resolution of the DInSAR observations and the shallow depth of the earthquake, it is reasonable to solve for a heterogeneous slip model [*Delouis et al.*, 2000].

In this study we combine previously published GPS and DInSAR data [*Stramondo et al.*, 1999; *Salvi et al.*, 2000] with additional DInSAR data from both ascending and descending ERS satellite passes (Plate 2) in a joint inversion to derive the coseismic slip distribution of the three main earthquakes of the 1997 Umbria-Marche sequence.

2. SAR Interferometry

Radar interferometry has emerged as an important tool for measuring coseismic surface displacements [*Massonnet et al.*, 1993; *Peltzer and Rosen*, 1995]. Repeat pass SAR interferometry is a technique that uses multiple radar images to calculate topography or surface change over the image area [e.g. *Gabriel et al.*, 1989; *Massonnet and Feigl*, 1998; *Rosen et al.*, 2000]. We generate differential interferograms from the European Remote Sensing satellites (ERS-1 and ERS-2) by differencing their phase and correcting for the effects of topography and Earth curvature [*Zebker and Goldstein*, 1986]. To subtract topography we used a digital elevation model (DEM) provided by the Italian Istituto Geografico Militare (IGM), produced from 1:25,000 topographic maps, with a 20 m pixel size and an estimated height resolution of about 25 m.

Due to the strong topographic relief of the Apennines and the significant vegetation cover (large deciduous forests and intensive agriculture) of the epicentral area, even the best interferograms show large decorrelation areas [*Salvi et al.*, 2000]. For this reason, even though a large number of SAR data are available from July 1993 to October 1997 (about 30 images) only three significant interferograms are shown in the two previous papers on this

earthquake sequence [Stramondo *et al.*, 1999; Salvi *et al.*, 2000] with temporal separation of the SAR images not exceeding 70 days.

In this study we use two interferograms previously analyzed in Stramondo *et al.* [1999], and in Salvi *et al.* [2000]. In Stramondo *et al.* [1999] they analyze the 35-day ERS-2 descending interferogram, altitude of ambiguity ($ha=65$ m), the error in the digital elevation model that will produce one phase cycle of error in the differential interferogram. This interferogram (Plate 2c) covers the period September 7 – October 12, 1997 (hereinafter the “Colfiorito interferogram”), and is the most coherent one available. Salvi *et al.* [2000] include the 70-day ($ha=65$ m) ERS-2-ERS-1 ascending interferogram that covers the time interval August 9 – October 17, 1997 (the “Colfiorito-Sellano interferogram”). It clearly shows a deformation pattern that extended toward the south due to the 14 October, Sellano event (Plate 2d). This interferogram represents the cumulative displacements from the three main events and their smaller aftershocks.

We compute an additional interferogram (Plate 2a) that isolates the deformation field relative to the Sellano main event from the two other mainshocks of the sequence (Table 1). It is obtained with a 35-day ($ha=39$ m) descending ERS-2 pair, October 12 – November 16 (hereinafter the “Sellano interferogram”). The pre-seismic image (Oct. 12) is the same post-seismic image used by Stramondo *et al.* [1999] for the Colfiorito descending satellite track interferogram (Plate 2c). Thus, the Colfiorito and Sellano interferograms show the displacement field relative to adjacent time intervals, September 7 – October 12 and October 12 – November 16, 1997.

The Sellano interferogram altitude of ambiguity is within the DEM resolution. In the Sellano interferogram there is a clear NW-SE trending, 13 km long by 6 km wide, fringe pattern. Notwithstanding the large vegetated zones and the strong topography that result in

low coherence areas, we recognize six phase cycles, corresponding to a maximum of -16.8 cm of range displacement (Plate 2b). The reported epicenter of the Sellano event is 1.5 km SW of this maximum deformation area.

3. GPS Data

The GPS displacements we use in this study are a subset of those presented in *Salvi et al.* [2000], based on the original GPS analysis [*Anzidei et al.*, 1999; *Hunstad et al.*, 1999]. We chose this subset to eliminate a few stations at greater distance from the earthquakes in this study and which also had negligible displacements. The GPS data are relative to stations of the IGM95 network, first measured in March-April 1995, and re-occupied in two different GPS campaigns after the Colfiorito and Sellano events. The values we use are for the stations listed in Table 2 and plotted in Figure 1. The accuracy of horizontal and vertical components for these data are 23-26 mm and 38-45 mm, respectively (*Anzidei et al.*, 1999).

4. Fault Modeling

To model the complex slip of the Umbria-Marche earthquake sequence distributed across multiple faults we use the method of simulated annealing, an iterative quasi-Monte Carlo global minimization algorithm that has been applied to modeling fault slip using GPS data [*Ihmle and Ruegg*, 1997; *Lundgren et al.*, 1999], and more recently for modeling combined seismic and DInSAR data sets [*Delouis et al.*, 2000].

The fault parameters used for the model (Table 3) are based on the CMT solutions (*Ekström et al.*, 1998) except for two differences. For the two events of September 26 we assume that the faults belong to the same structure and use a common strike of 143° . Instead, for the Sellano event the best fit between the data and model was obtained assuming a strike

of 135° (strike 122° for the CMT solution) which is required by the strike of the high fringe-rate up-dip edge of the deformation pattern [see also *Salvi et al.*, 2000].

In our application of this approach we discretize a fault plane with a specified geometry and dimensions into a grid of rectangular subfaults in an elastic half-space with surface displacements calculated using the dislocation equations of *Okada* [1985, 1992]. We use fault patches with dimensions of 2.25×2 km and 3×2 km for the lengths and widths of the Colfiorito and Sellano faults, respectively. Thus constrained, we solve for the slip magnitude and direction on each patch.

For this study we seek the model that best fits both the GPS data and the contoured DInSAR data from three different interferograms. In addition, we can also seek to constrain the solution to match the total seismic scalar moment observed for the earthquake sequence. All rms misfits between observations (whether surface motions or total moment) and the model are individually computed, scaled by a weighting factor, and summed to compute the total “cost” of a particular solution.

The DInSAR data contours are from three interferograms, one covering the entire September to October earthquake sequence on an ascending interferogram, the other two interferograms formed from descending data covering the Colfiorito and Sellano areas separately. Since the data consist of relative phase contours a phase bias for each set of contours must be estimated for the solution. For the ascending interferogram the Colfiorito and Sellano fringe patterns are partially joined, thus linking the two areas to within a common phase offset and linking the two descending sets of DInSAR data through the joint inversion; a point that will become important later in the comparison of the inversion results with seismologically derived earthquake parameters. In our simulated annealing solutions we have assigned a standard deviation of 10 mm to each contoured data point. The DInSAR data

only provide a picture of the deformation projected into the satellite radar line-of-sight (approximately 23° from the vertical at mid-swath). By using both ascending and descending data (which look from roughly the west and east, respectively) we increase our sensitivity to the horizontal (essentially E-W) surface displacements.

We explored a range of solutions through variations in the weighting of the different data. We present the results for two cases, Model A, constrained only by the DInSAR data and M_0 , the total seismic moment (weight SAR 10, weight GPS, 0; weight M_0 , 10^{-31}) shown in Plate 3; and, Model B, in which the costs of the DInSAR and GPS data are approximately the same (weight GPS, 2000; weight SAR, 10), in addition to the total seismic moment constraint (weight M_0 , 10^{-31}), placed on the modeled slip (Plate 4). The weights for the three different constraints were determined in order to balance the cost contribution of each constraint (i.e. the larger weight of the GPS relative to the DInSAR data for Model B produced a similar cost contribution from each for similar fits to the respective data sets). In Plates 3 and 4 the DInSAR data are represented as an image of points through a bicubic interpolation for visualization purposes only.

In each case the slip magnitude for each fault patch is allowed to fall within the range of 0-3000 mm, and the rake angle can vary from -90 to 0 degrees (pure normal slip to pure left-lateral strike-slip). Three separate phase offsets were also estimated, each allowed to fall in the range of -28 to $+28$ mm. For Model A, the solution was rather insensitive to the phase offsets, and solution values for the three sets of phase contours shown in Plate 2*b,c,d* were 0, 4, and 1 mm, respectively. For Model B the phase offsets were -2 , 11, and -3 mm, respectively.

A number of other model constraints and weights were explored in addition to those presented here. We present the results from two end-members that illustrate the relative

contributions of the two geodetic data sets and scalar moment constraint on the fault slip solution. The two cases we present here represent members from the least constrained (only the DInSAR data and scalar moment constraint Model A - a minimum data set for trying to image the fault slip distribution), to a model constrained by all the relevant information available in this study (Model B). Among the other cases examined, we had initially constrained the solution to pure normal fault slip (rake equal to -90°). The solution for this model was not able to fit the strike-parallel component of horizontal displacement found at GPS site CROC, in particular. Only with the allowance of a left-lateral strike-slip component were the solutions able to match the observed GPS vectors. With the allowance of strike-slip motion, different weights were explored. Models in which both the DInSAR and GPS data were constrained but the scalar moment weight was set to zero produced a slip pattern that was essentially intermediate between that of Models A and B.

5. Discussion and Conclusions

The following observations can be made from the inversion results. 1) Allowing only dip-slip in the model could not produce a reasonable fit to the horizontal displacement vector at GPS site CROC. 2) Allowing strike-slip motion and only fitting the ascending and descending DInSAR data (Plate 1), the inversion computes a strike-slip component of motion that partially fits the strike-slip component of motion at GPS site CROC. 3) By including the GPS data in the solution we find a similar solution but with an improved fit to the GPS as would be expected (Plate 4). 4) The main discrepancy with this model and observations lies in the value for the total scalar moment, M_0 , for the Sellano segment. Models in which this value was constrained to sum to the value for the sum of the M_0 for the six largest events between September 26 and October 14, 1997 (2.3×10^{18} N-m) produced a scalar moment

total slightly higher (2.5×10^{18} N-m) than the seismic value. The discrepancy arises when we compare the value for the Sellano segment (0.8×10^{18} N-m), nearly double the total scalar seismic moment (0.42×10^{18} N-m) observed. A similar result was found by *Salvi et al.* [2000] for the Sellano event. As part of the procedure for inverting the DInSAR data we allow for a phase bias of ± 28 mm (one interferometric fringe). In these inversions the magnitude of the phase bias values estimated by the inversion have generally been less than 10 mm. In the case of the GPS data there is no such ambiguity, although the number of GPS points is small, thus placing a high importance on a few individual sites. GPS site PENN has an observed vertical displacement that is negative, a direction incompatible with the seismically constrained fault deformation models and with its own NE directed horizontal motion, which is in agreement with the fault dislocation models. For the solutions (Models A and B) the uncertainty for the PENN vertical component was set very large (10^6 mm) to minimize its effect on the solution, although leaving it at its nominal uncertainty did not affect the model results.

The general pattern of coseismic slip found is very similar in each case. The Colfiorito segment has most of the dip-slip concentrated along the middle of the modeled fault plane at a depth of 4.2-5.7 km. For the Sellano segment, dip-slip is concentrated over a single area over a depth range of 3.5-6.3 km. The most significant strike-slip motion is found at the SE end of the Colfiorito segment. It was robust across all solutions, whether considering the GPS data, or not. This is important since it demonstrates the need for a strike-slip component from two different types of geodetic data and it shows how DInSAR data from ascending and descending images can be combined to resolve the strike-slip component which in this case is largely a function of sensitivity to horizontal displacements.

The results of our inversion are generally in agreement with the combined DInSAR, GPS, and strong motion models of *Hernandez et al.* [2000]. Differences in the fault parameters, crustal structure, and inversion method result in differences in the details of the slip, as well as the restriction to purely normal slip for their models. In their study ascending and descending DInSAR data were used to constrain the two September 26, 1997, earthquakes (equivalent to our Plate 2c,d), and only contours for the ascending interferogram covering the Sellano event (equivalent to our Plate 2d) were used in their inversion. The use of GPS data in this study and that of *Hernandez et al.* [2000] was also somewhat different. They used slightly more sites (generally farther away), yet they essentially weighted the vertical components to zero. Effects can also be expected due to differences in the assumed near source structure. In this study we use the analytical formulations of *Okada* [1985] for an elastic halfspace, whereas the *Hernandez et al.* [2000] study allows for a layered halfspace, which is especially important for their strong motion modeling, but which also effects the calculated ground displacements for the geodetic data [*Savage*, 1998; *Cattin et al.*, 1999], mainly through error in the apparent depth of the source in the halfspace. A significant difference is found in the calculated amplitudes of the highest slip. Our maximum slips for both the Colfiorito (UTC 9:40 event) and the Sellano event were on the order of 2 meters, compared to 1 meter maximum in the *Hernandez et al.* [2000] study. For solutions in which the weight of the total seismic moment was increased, there was a reduction in the slip on the Sellano segment to a maximum of ~1 meter, but at the expense of having a poorer fit to the DInSAR data.

In Model B, slip is concentrated on areas of relatively high amplitude over ~0.5 m with slip locally reaching 2 m. The static stress drop for a rectangular fault can be calculated from [*Kanamori and Anderson*, 1975]:

$$\Delta\sigma=2\mu u/W\pi$$

where $\mu = 3 \times 10^{10}$ Pa, u is the slip, and $W = 2$ km is the width. For the slip magnitudes calculated in Model B (Plate 4), the maximum stress drops for each fault are approximately 20 MPa with average stress drops over the areas exceeding 0.4 m slip approximately 10 MPa on each fault. Notwithstanding the possible biases in our slip amplitudes due to the simplicity of our crustal model, the highest stress drops are high compared with estimates of 2-10 MPa for stress drops estimated from earthquake slip [Smith and Priestley, 2000; Venkataraman *et al.*, 2000] or microseismicity [Rubin and Gillard, 2000] in California, although $\Delta\sigma > 50$ MPa have been estimated for individual asperities on one of these events [Pacheco and Nabelek, 1988]. The highest stress drops we estimate for the individual patches (20 MPa) agrees with estimates based on strong motion data for the September 26, 1997, Colfiorito sequence of 20 MPa [Castro *et al.*, 2000; Malagnini and Herrmann, 2000].

The current static image of the fault slip does not address the issue of earthquake triggering, especially with regard to the Sellano earthquake. The slip distribution we calculate fits a pattern of two side-by-side centers of slip on the Colfiorito segment and one area of concentrated slip on the Sellano segment. Each of these high slip areas lies near one of the three main earthquakes in this sequence. Continuation of slip toward the SE end of the Colfiorito segment is suggested by the model. As shown for the 1999 Izmit, Turkey earthquake, rupture propagation can continue through areas of lower slip [Delouis *et al.*, 2000]. Slip on the SE end of the Colfiorito segment, whether coseismic or postseismic afterslip, apparently was limited by the structural interruption of that fault segment.

From a model for the static coseismic slip (Plate 4) for the Colfiorito segment that ruptured during the September 26, 1997 events, we can see that the Coulomb stress change [King *et al.*, 1994; Toda *et al.*, 1998] for the geometry and mechanism of the Sellano

earthquake lies in a positive lobe, both in map view at the center depth of the fault rupture, and in cross section (Plate 5). A model for the Coulomb stress in which the Colfiorito segment is treated as a homogeneous, normal slipping fault yields a similar pattern (although the actual area of the Sellano fault in the cross section is reduced in stress amplitude). This is similar to the static stress change model computed for this earthquake sequence by *Cocco et al.* [2000]. Clearly models such as these can yield insight into where subsequent earthquakes are more likely to occur [*e.g. Hodgkinson et al.*, 1996; *Parsons et al.*, 2000], and the Sellano earthquake fits this model, however, the timescale of fault interactions cannot be addressed from the slip distribution alone [*Belardinelli et al.*, 1999]. Dynamic stress changes affecting crack growth both near and distant the primary earthquake must be considered in understanding the interaction between related events [*Brodsky et al.*, 2000].

This study represents a step forward toward combining all the relevant geodetic data available for the 1997 Umbria-Marche earthquake sequence. We solve for the distribution of slip and change in slip direction over the two main planes representing coseismic slip of the three largest earthquakes. Both the GPS and DInSAR data are fit with similar models which show that combining both ascending and descending DInSAR data give similar horizontal surface displacements. We find that dip-slip is mostly concentrated in a fairly narrow depth range 2-6 km for both earthquakes, with most of the strike-slip motion located toward the southern end of the Colfiorito fault structure. Coulomb stress calculations show that slip on the Colfiorito fault plane acted positively toward triggering slip on the Sellano fault.

References

- Amato, A., R. Azzara, C. Chiarabba, et al., The Colfiorito, Umbria-Marche earthquake sequence in central Italy (Sept.-Nov., 1997): A first look to mainshocks and aftershocks, *Geophys. Res. Lett.*, 25, 2861-2864, 1998.
- Anzidei, M., P. Baldi, A. Galvani, A. Pesci, I. Hunstad, and E. Boschi, Coseismic displacement of the 27th September 1997 Umbria-Marche (Italy) earthquakes detected by GPS: Campaigns and data, *Ann. Geofis.*, 42, 597-607, 1999.
- Basili, R., V. Bosi, F. Galadini, P. Galli, M. Meghraoui, P. Messina, M. Moro, and A. Sposato, The Colfiorito earthquake sequence of September-October 1998: Surface breaks and seismotectonic implications for the central Apennines (Italy), *J. Earthquake Eng.*, 2, 1-12, 1998.
- Belardinelli, M. E., M. Cocco, O. Coutant, and F. Cotton, Redistribution of dynamic stress during coseismic ruptures: Evidence for fault interaction and earthquake triggering, *J. Geophys. Res.*, 104, 14,925-14,945, 1999.
- Brodsky, E. E., V. Karakostas, and H. Kanamori, A new observation of dynamically triggered regional seismicity: Earthquakes in Greece following the August, 1999 Izmit, Turkey earthquake, *Geophys. Res. Lett.*, 27, 2741-2744, 2000.
- Castro, R. R., A. Rovelli, M. Cocco, F. Pacor, and M. Di Bona, Stochastic simulation of strong-motion records from the September 26, 1997 ($M_w = 6$) Umbria-Marche (central Italy) earthquake, *Bull. Seism. Soc. Am.*, submitted, 2000.
- Cattin, R., P. Briole, H. Lyon-Caen, P. Bernard, and P. Pinettes, Effects of superficial layers on coseismic displacements for dip-slip faults and geophysical implications, *Geophys. J. Int.*, 137, 149-158, 1999.

- Cello, G., S. Mazzoli, E. Tondi, and E. Turco, Active tectonics of the central Apennines and possible implication for seismic hazard analysis in peninsular Italy, *Tectonophysics*, 272, 43-60, 1997.
- Cinti, F. R., L. Cucci, F. Marra, and P. Montone, The 1997 Umbria-Marche (Italy) sequence: Relationship between ground deformation and seismogenic structure, *Geophys. Res. Lett.*, 26, 895-898, 1999.
- Cocco, M., C. Nostro, and G. Ekström, Static stress changes and fault interaction during the 1997 Umbria-Marche earthquake sequence, *J. Seismol.*, in press, 2000.
- Delouis, B., P. Lundgren, J. Salichon, and D. Giardini, Joint inversion of InSAR and teleseismic data for the slip history of the 1999 Izmit (Turkey) earthquake, *Geophys. Res. Lett.*, 27, 3389-3392, 2000.
- Ekström, G., A. Morelli, E. Boschi, and A. M. Dziewonski, Moment tensor analysis of the central Italy earthquake sequence of September-October 1997, *Geophys. Res. Lett.*, 25, 1971-1974, 1998.
- Gabriel, A., R. Goldstein, and H. Zebker, Mapping small elevation changes over large areas: Differential radar interferometry, *J. Geophys. Res.*, 94, 9183-9191, 1989.
- Hernandez, B., F. Cotton, M. Campillo, F. Courboulex, M. Cocco, and S. Stramondo, Rupture history of the 1997 Umbria-Marche (central Italy) largest earthquakes from inversion of GPS, DInSAR and near field seismological data, *J. Geophys. Res.*, submitted, 2000.
- Hodgkinson, K. M., R. S. Stein, and G. C. King, The 1954 Rainbow Mountain-Fairview Peak-Dixie Valley earthquakes: A triggered normal faulting sequence, *J. Geophys. Res.*, 101, 25,459-25,471, 1996.

- Hunstad, I., M. Anzidei, M. Cocco, P. Baldi, A. Galvani, and A. Pesci, Modelling coseismic displacements during the 1997 Umbria-Marche earthquake (central Italy), *Geoph. J. Int.*, *139*, 283-295, 1999.
- Ihmle, P. F., and J.-C. Ruegg, Source tomography by simulated annealing using broad-band surface waves and geodetic data: Application to the $M_w = 8.1$ Chile 1995 event, *Geophys. J. Int.*, *131*, 146-158, 1997.
- Kanamori, H., and D. Anderson, Theoretical basis of some empirical relations in seismology, *Bull. Seism. Soc. Am.*, *65*, 1073-1075, 1975.
- King, G. C. P., R. S. Stein, and J. Lin, Stress changes and the triggering of earthquakes, *Bull. Seism. Soc. Am.*, *84*, 935-953, 1994.
- Lundgren, P., M. Protti, A. Donnellan, M. Heflin, E. Hernandez, and D. Jefferson, Seismic cycle and plate margin deformation in Costa Rica: GPS observations from 1994 to 1997, *J. Geophys. Res.*, *104*, 28915-28926, 1999.
- Malagnini, L., and R. B. Herrmann, Ground-motion scaling in the region of the 1997 Umbria-Marche earthquake (Italy), *Bull. Seism. Soc. Am.*, *90*, 1041-1051, 2000.
- Massonnet, D., M. Rossi, C. Carmona, F. Adragna, G. Peltzer, K. Feigl, and T. Rabaute, The displacement field of the Landers earthquake mapped by radar interferometry, *Nature*, *364*, 138-142, 1993.
- Massonnet, D., and K. Feigl, Radar interferometry and its application to changes in the Earth's surface, *Rev. Geophys.*, *36*, 441-500, 1998.
- Okada, Y., Surface deformation due to shear and tensile faults in a half-space, *Bull. Seism. Soc. Am.*, *75*, 1135-1154, 1985.
- Okada, Y., Internal deformation due to shear and tensile faults in a half-space, *Bull. Seism. Soc. Am.*, *82*, 1018-1040, 1992.

- Pacheco, J., and J. Nabelek, Source mechanisms of three moderate California earthquakes of July 1986, *Bull. Seism. Soc. Am.*, 78, 1907-1929, 1988.
- Parsons, T., S. Toda, R. Stein, A. Barka, and J. Dieterich, Heightened odds of large earthquakes near Istanbul: An interaction-based probability calculation, *Science*, 288, 661-665, 2000.
- Peltzer, G., and P. Rosen, Surface displacement of the 17 May 1993 Eureka Valley, California, earthquake observed by SAR interferometry, *Science*, 268, 1333-1336, 1995.
- Rosen, P. A., S. Hensley, I. R. Joughin, F. K. Li, S. N. Madsen, E. Rodriguez, and R. M. Goldstein, Synthetic aperture radar interferometry, *Proc. IEEE*, 88, 333-382, 2000.
- Rubin, A. M., and D. Gillard, Aftershock asymmetry/rupture directivity among central San Andreas fault microearthquakes, *J. Geophys. Res.*, 105, 19,095-19,109, 2000.
- Salvi, S., S. Stramondo, M. Cocco, M. Tesauro, I. Hunstad, M. Anzidei, P. Briole, P. Baldi, E. Sansosti, G. Fornaro, R. Lanari, R. Doumaz, A. Pesci, and A. Galvani, Modeling coseismic displacements resulting from SAR interferometry and GPS measurements during the 1997 Umbria-Marche seismic sequence, *J. Seismol.*, 4, 479-499, 2000.
- Savage, J. C., Displacement field for an edge dislocation in a layered halfspace, *J. Geophys. Res.*, 103, 2439-2446, 1998.
- Smith, K. D., and K. F. Priestley, Faulting of the 1986 Chalfant, California, sequence: Local tectonics and earthquake source parameters, *Bull. Seism. Soc. Am.*, 90, 813-831, 2000.
- Stramondo, S., M. Tesauro, P. Briole, E. Sansosti, S. Salvi, R. Lanari, M. Anzidei, P. Baldi, A. Avallone, M. F. Buongiorno, G. Franceschetti, and E. Boschi, The September 26, 1997 Colfiorito, Italy, earthquakes: Modeled coseismic surface displacement from SAR interferometry and GPS, *Geophys. Res. Lett.*, 26, 883-886, 1999.

Toda, S., R. S. Stein, P. A. Reasenberg, J. H. Dieterich, and A. Yoshida, Stress transferred by the 1995 Mw=6.9 Kobe, Japan, shock: Effect on aftershocks and future earthquake probabilities, *J. Geophys. Res.*, 103, 24543-24565, 1998.

Venkataraman, A., J. Mori, H. Kanamori, and L. Zhu, Fine structure of the rupture zone of the April 26 and 27, 1997, Northridge aftershocks, *J. Geophys. Res.*, 105, 19,085-19,093, 2000.

Zebker, H. A., and R. M. Goldstein, Topographic mapping from interferometric SAR observations, *J. Geophys. Res.*, 91, 4993-5001, 1986.

Tables

Table 1. Source parameters of the moderate-magnitude events of the 1997 Umbria-Marche seismic sequence.

| No. | Event | Lat. ^{a,b,c} | Long. ^{a,b,c} | D ^{a,b,c} (km) | M_l ^a | M_w ^d | M_0 ^d (* 10^{18} N-m) | Strike, dip, rake ^d (°) |
|-----|---------|-----------------------|------------------------|------------------------------|--------------------|--------------------|---|---------------------------------------|
| 1 | 970926a | 43.° 01.20' | 12.°53.30' | 6.5 | 5.6 | 5.7 | 0.40 | 152, 46, -83 |
| 2 | 970926b | 43.° 01.82' | 12.°51.51' | 6.0 | 5.8 | 6.0 | 1.20 | 144, 42, -80 |
| 3 | 971003 | 43.° 02.06' | 12.°50.14' | 5.0 | 5.0 | 5.2 | 0.09 | 141, 43, -74 |
| 4 | 971006 | 43.° 01.04' | 12.°50.17' | 5.5 | 5.4 | 5.4 | 0.17 | 145, 40, -80 |
| 5 | 971012 | 42.° 54.78' | 12.°56.76' | 5.0 | 5.1 | 5.2 | 0.08 | 154, 51, -82 |
| 6 | 971014 | 42.° 55.26' | 12.°55.51' | 5.5 | 5.5 | 5.6 | 0.34 | 122, 38, -100 |

^a Amato et al., 1998.

^b C. Chiarabba, written communication, 1999.

^c M. Di Bona, written communication, 1999.

^d Ekström et al., 1998.

^e Pino et al., 1998; Pino and Mazza, 1999.

Table 2 - Coseismic displacement at the GPS stations used in this study, from *Salvi et al.* [2000].

| Station | N (mm) | σ_N (mm) | E (mm) | σ_E (mm) | V (mm) | σ_V (mm) |
|---------|--------|-----------------|--------|-----------------|--------|-----------------|
| COLF | -9.7 | 23 | 14.2 | 23 | -64.8 | 38 |
| CROC | -144.4 | 23 | -14.6 | 23 | -243.3 | 45 |
| CAPA | -61.6 | 23 | 12.9 | 23 | 2.9 | 45 |
| FOLI | -40.5 | 23 | -34.8 | 23 | 35.2 | 40 |
| GAIF | -9.1 | 23 | 41.2 | 23 | 18.9 | 45 |
| OGAT | -7.1 | 23 | 43.6 | 23 | 40.3 | 38 |
| PENN | 70.2 | 26 | 85.4 | 26 | -34.8 | 45 |
| RIVO | -22.9 | 23 | -14.7 | 23 | -19.6 | 41 |

Table 3. Model fault geometry parameters* for solutions shown in Plates 3 and 4.

| <i>Segment</i> | <i>L (km)</i> | <i>W (km)</i> | <i>D (km)</i> | <i>Strike(°)</i> | <i>Dip(°)</i> | ΔL (km) | ΔW (km) |
|----------------|---------------|---------------|---------------|------------------|---------------|-----------------|-----------------|
| Colfiorito | 18 | 10 | 7.11 | 143 | 45 | 2.25 | 2 |
| Sellano | 12 | 8 | 6.3 | 135 | 45 | 3 | 2 |

*Fault parameters are for the faults outlined in Plate 1. L is the overall length of each fault, W the width, D the depth to the bottom of the fault in the convention of *Okada* [1985]. ΔL and ΔW are the length and width of the fault patches for each fault segment.

Figure Captions

Figure 1. Comparison of GPS data (solid black arrows) vectors used in this study [*Salvi et al.*, 2000] with the modeled solutions: gray filled arrows are for Model A, no GPS constraint; white filled arrows are for Model B, constrained by DInSAR, and GPS data, plus the total seismic moment.

Plate 1. Shaded relief map showing the focal mechanisms of the main earthquakes (1- M_w 6.0 09:40 09/26/97; 2- M_w 5.7 00:33 09/26/97; 3- M_w 5.6 10/14/97). The boxes outline the faults used in Models A and B, and shown in Plates 3-5.

Plate 2. DInSAR data used in this study. Orange dots correspond to the 6 earthquakes listed in Table 1. *a)* Differential interferogram for the Sellano event. DInSAR data were calculated from ERS data acquired on 10/12/97 – 11/16/97 with a perpendicular baseline separation of 200 m. *b)* Contoured descending data from (*a*). Both panels (*a*) and (*b*) have the same map

scale, slightly different from the map scale for panels (c) and (d). c) Contoured descending track interferograms for the Colfiorito segment 09/07/97-10/12/97 [Salvi *et al.*, 2000]. d) Contoured ascending data for the 08/09/97-10/17/97 interferogram [Salvi *et al.*, 2000]. Scale bar refers to the interferogram contours at 28 mm intervals (relative to an overall constant shift). Contours for each panel (b,c,d) have independent unknown constant shifts.

Plate 3. Simulated annealing solution for Model A, constrained by the DInSAR data and the total seismic moment. a) Bicubic interpolation of the ascending data shown in Plate 2b. The black arrow in the lower left shows the radar look direction. b) Ascending InSAR model (bicubic interpolation) and comparison of observed horizontal GPS (black, open arrows) with modeled horizontal GPS vectors (green, open arrows). A 100 mm arrow is shown for scale at the bottom. c) Residual fit (observed-model) to the ascending DInSAR data. d) Descending interpolated InSAR data (from contours shown in Plate 2c). The black arrow in the lower left shows the radar look direction. e) Descending DInSAR model (interpolated) and observed (black arrows) and modeled (green arrows) GPS vertical displacements. GPS vectors are at the same scale as the horizontal vectors in (b). f) Residual fit to the descending DInSAR data. g) Fault motion model. Colors represent the slip magnitude, solid black arrows show the slip direction of the hanging wall relative to the foot wall of the fault. Slip convention is that of Okada [1985] Small white squares show the locations of the three main earthquakes.

Plate 4. Simulated annealing solution for Model B, constrained by the DInSAR, GPS, and total seismic moment. Panels a-g are as described for Plate 3a-g.

Plate 5. Coulomb static stress calculation for the slip of Model B (Plate 4) using the computer program Coulomb 1.3 [Toda *et al.*, 1998]. Coulomb stress is computed for the fault geometry of the Sellano fault modeled in this study assuming pure normal dip-slip motion and a coefficient of friction of 0.4 [King *et al.*, 1994]. Red areas increase the likelihood of slip on faults with the same geometry as the Sellano fault. *a)* Map view at 3.5 km depth. *b)* Vertical cross section parallel the black line shown in (*a*).

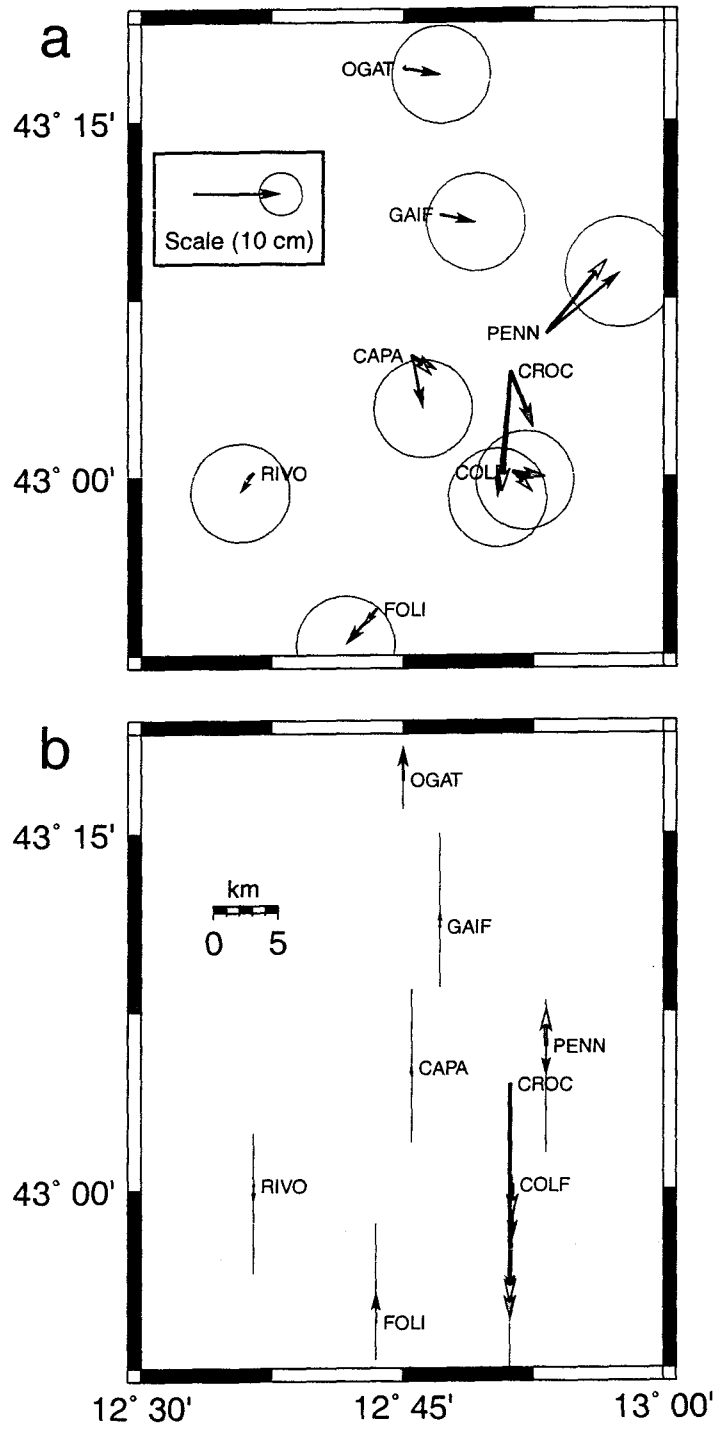


Figure 1

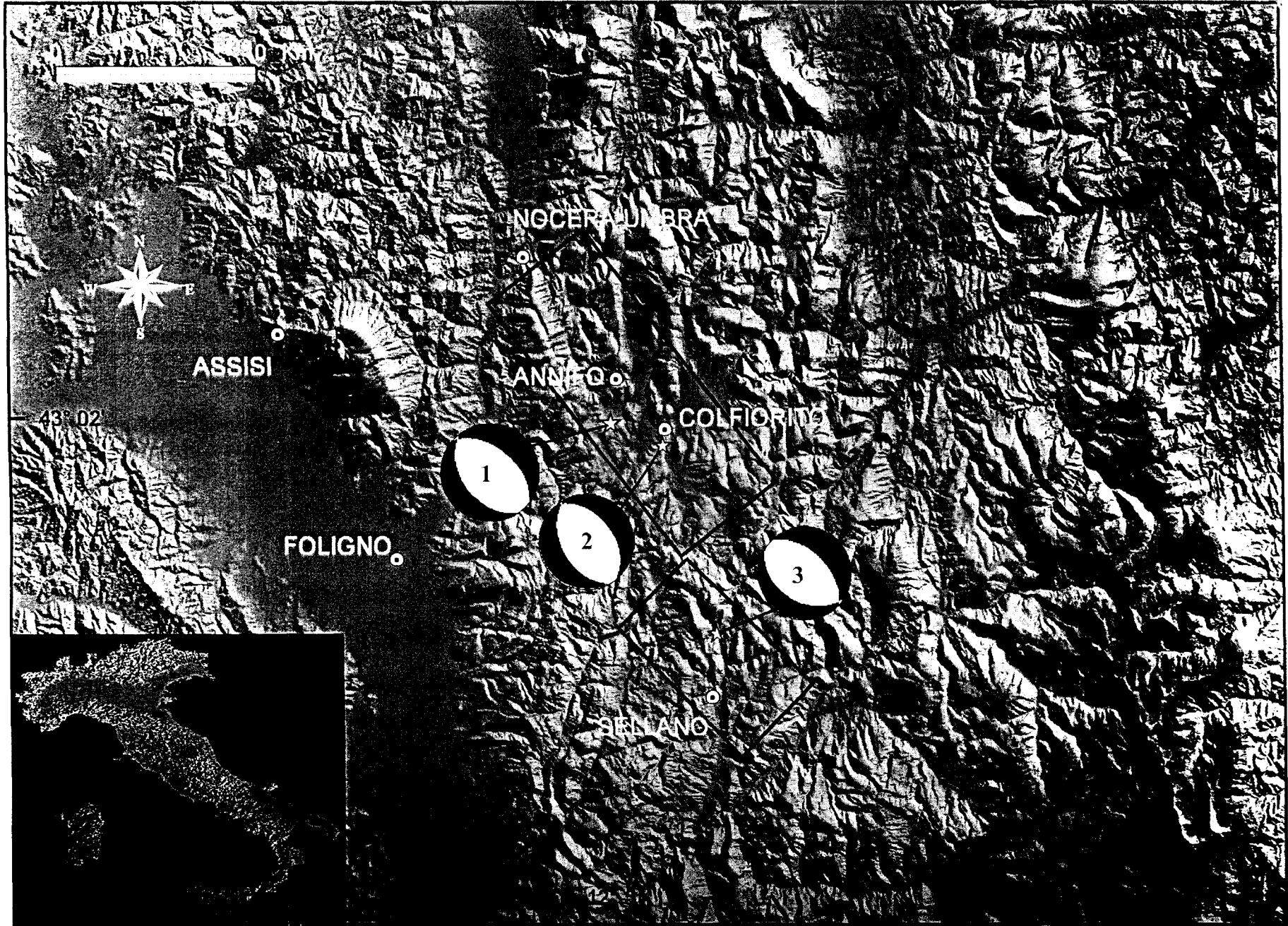
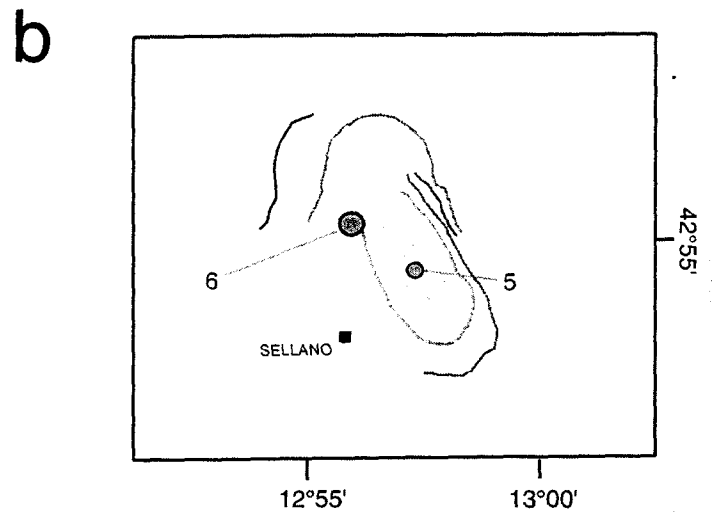
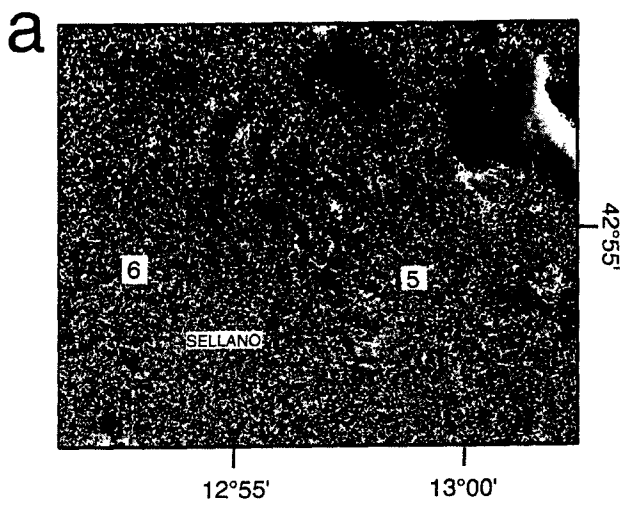
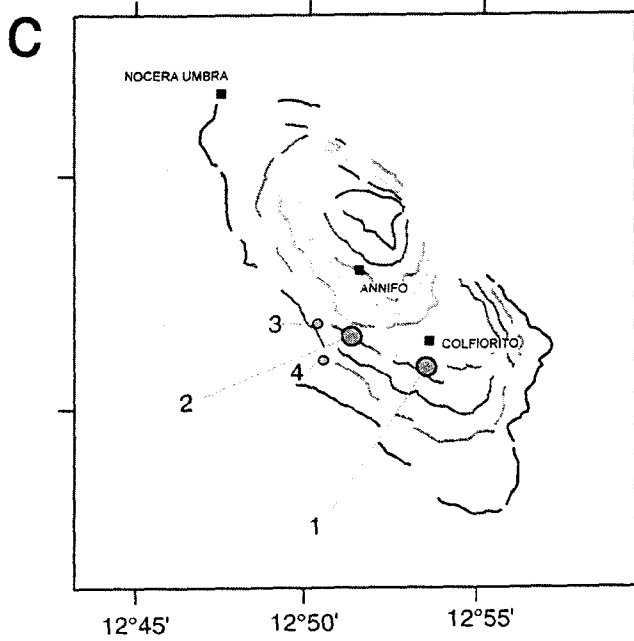


Plate 1 Lundgren and Stramondo

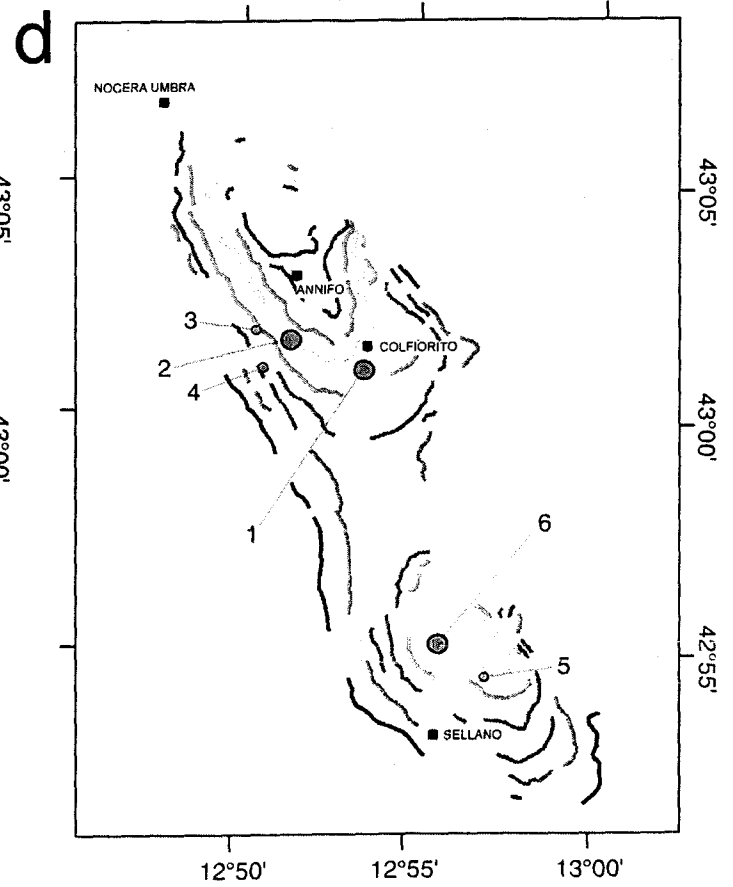


0 9 km

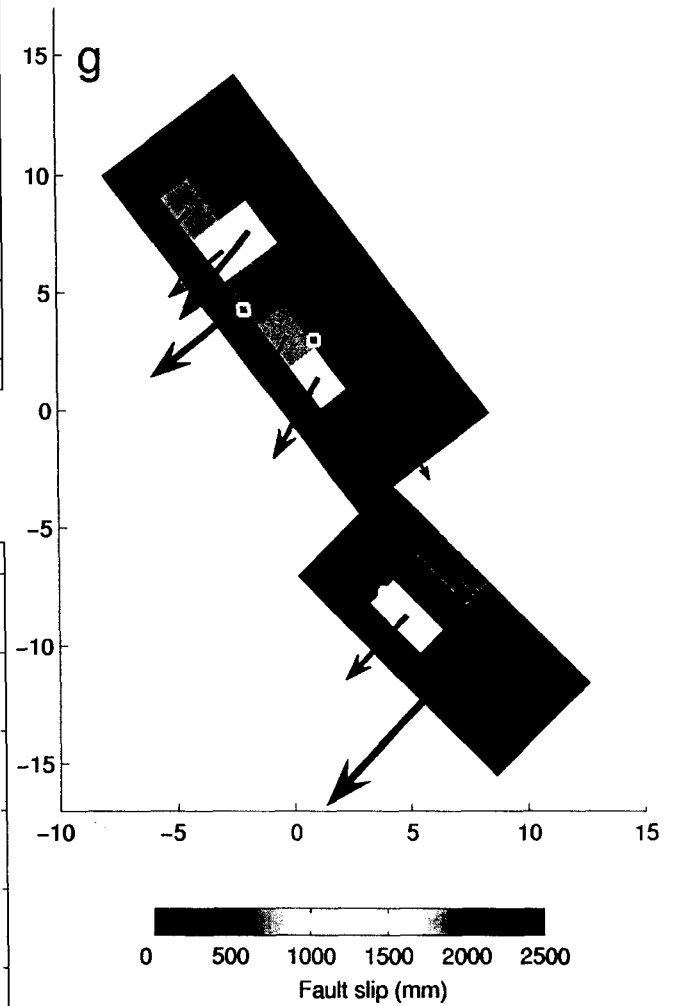
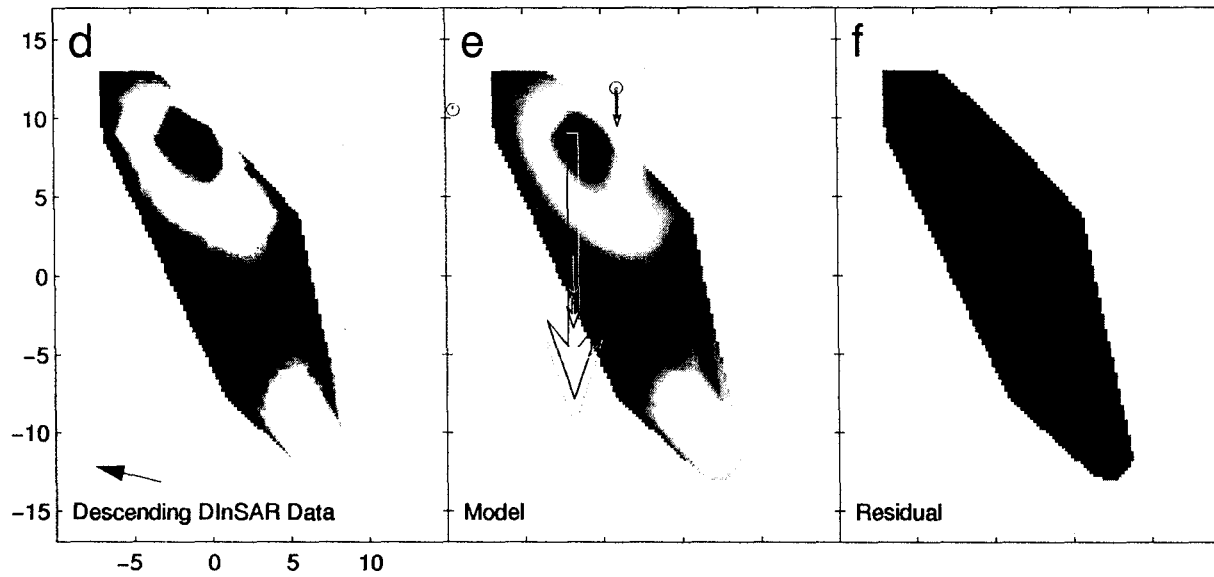
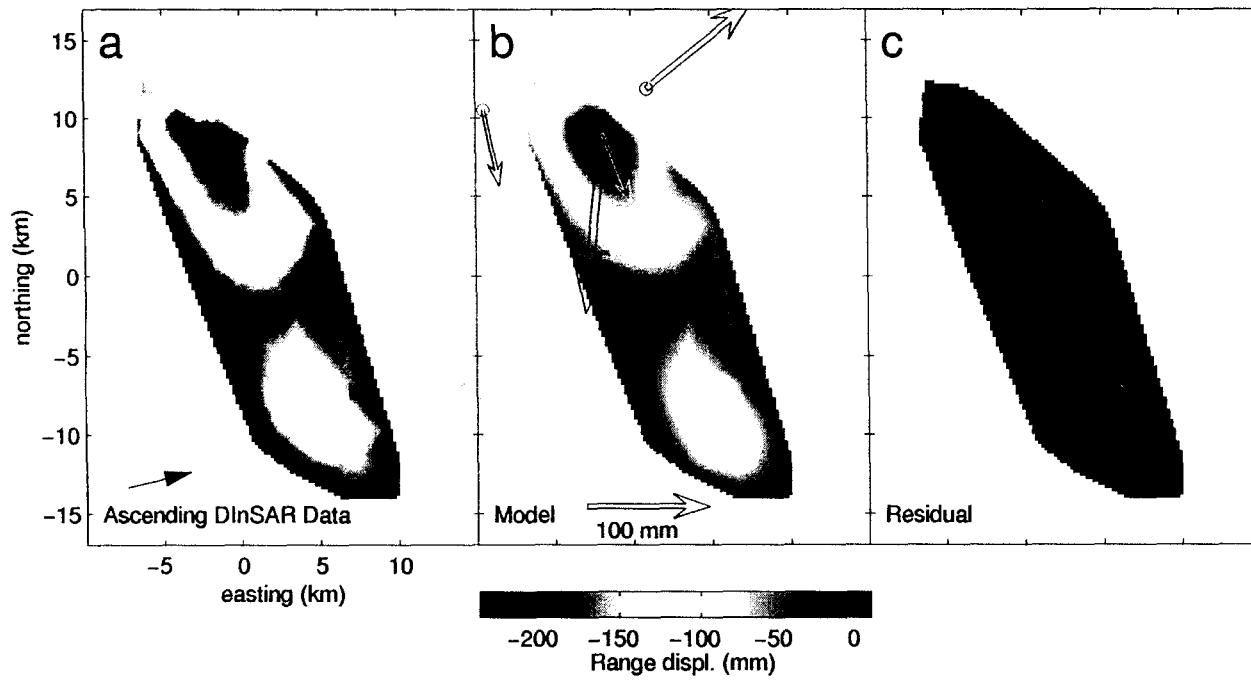


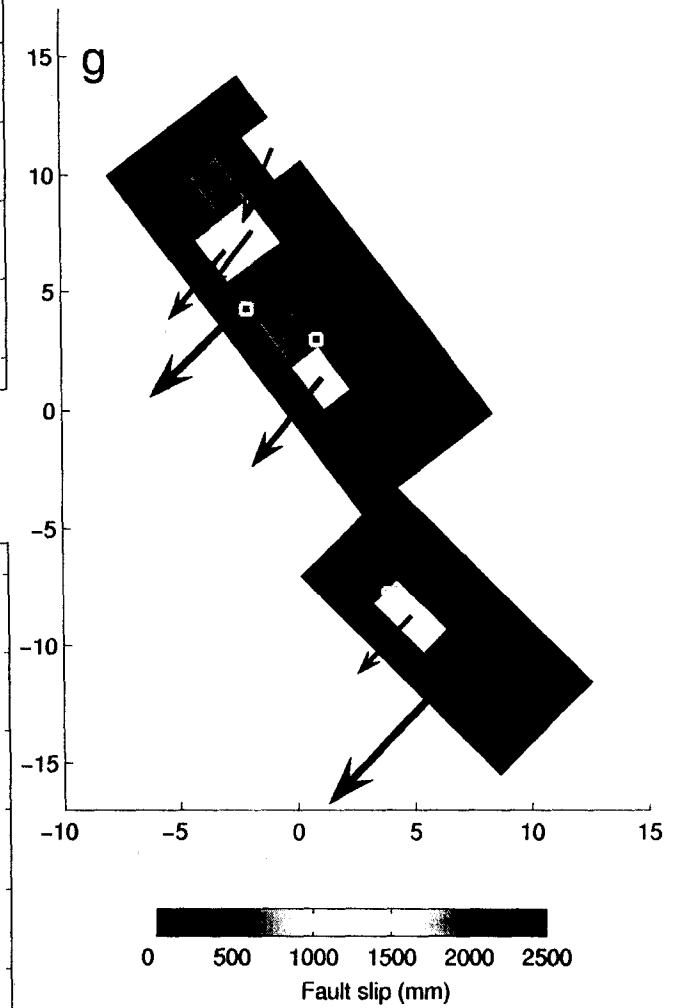
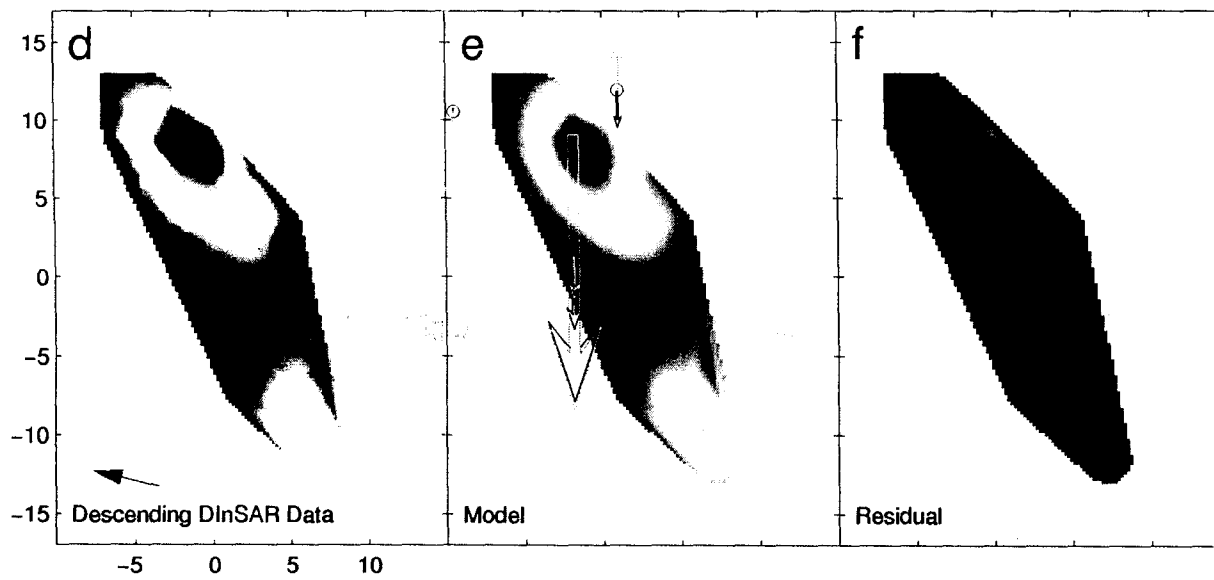
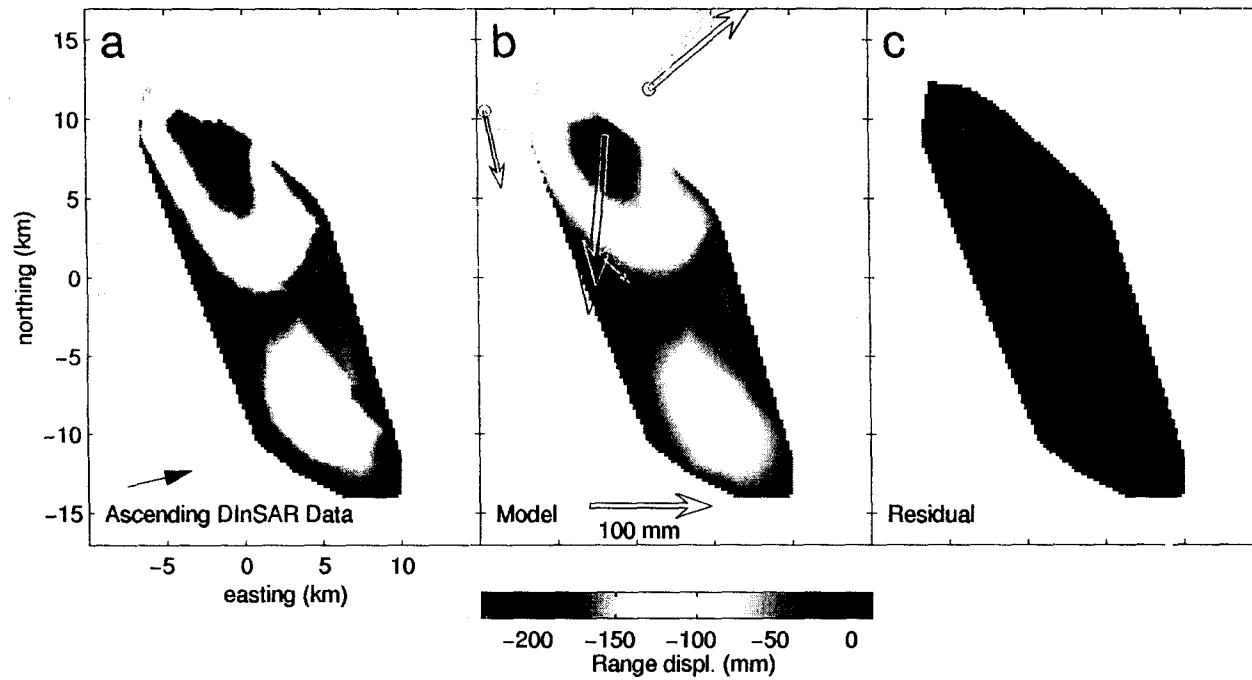
-224 -112 0

range contours (mm)



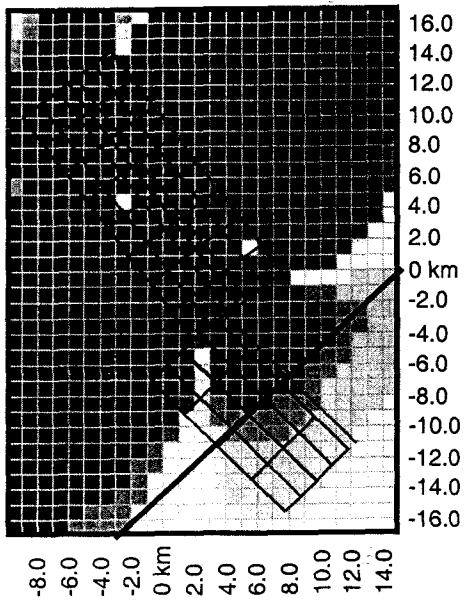
0 9 km





a

Mapview
depth 3.5 km



b

Cross-section

